Editors' Suggestion

Surface plasmon driven enhancement of linear and nonlinear magneto-optical Kerr effects in bimetallic magnetoplasmonic crystals in conical diffraction

V. B. Novikov,[1,*] A. M. Romashkina,[1] D. A. Ezenkova,[2,3] I. A. Rodionov,[2,3]
K. N. Afanasyev,[2,4] A. V. Baryshev,[2] and T. V. Murzina[1]
[1]*Department of Physics, Lomonosov Moscow State University, Moscow, 119991 Russia*
[2]*Dukhov Research Institute of Automatics (VNIIA), Moscow, 127055, Russia*
[3]*Bauman Moscow State Technical University, Moscow, 105005, Russia*
[4]*Institute for Theoretical and Applied Electrodynamics of Russian Academy of Sciences, Moscow, 125412, Russia*

(Received 20 December 2021; revised 29 March 2022; accepted 30 March 2022; published 12 April 2022)

Plasmonic crystals are an important backbone of modern photonics offering versatile control of light via manipulation of surface plasmon polaritons (SPPs). In particular, they sustain resonant light localization near the metal surface resulting in the enhancement of magneto-optical effects and nonlinear optical phenomena, the bridge of which is appealing for sensing and light routing. In this work we investigate the resonant SPP-driven enhancement of the transverse magneto-optical Kerr effect and the second harmonic generation under the conical diffraction of light in a one-dimensional magnetoplasmonic crystal (MPC) based on the combination of gold and ferromagnetic permalloy films. We demonstrate an extra way for the control over the magneto-optical effects in the MPC via the magnetic anisotropy of corrugated ferromagnetic film in the structure of the MPC.

DOI: 10.1103/PhysRevB.105.155408

I. INTRODUCTION

Resonant optical systems elicit huge research activity in modern photonics in view of their abundant applications for the manipulation of light. It stimulates high interest in plasmonic structures supporting resonant localization of light at subwavelength scales that found success in sensing [1–3], enhancement of light matter-interaction [4], and even lasing [5]. Special attention is attracted to surface plasmon polaritons (SPPs), which are the propagating surface light waves strongly localized at the metal/dielectric interface [6,7]. For the two juxtaposed dielectric and metal semispaces with the permittivities of ε_d and ε_m, respectively, the wave vector of the SPP is given by the following relation:

$$k_{\mathrm{SPP}} = k_0\sqrt{\frac{\varepsilon_d\varepsilon_m}{\varepsilon_d+\varepsilon_m}}, \tag{1}$$

where k_0 is the vacuum wave number [7]. Accordingly, the SPP dispersion is placed out of the light cone of a dielectric and requires the endfire [8,9], prism-based [10,11], or grating-based methods for the SPP excitation [12]. Relevant resonant enhancement of the electromagnetic field stimulates interest for plasmonic crystals (PCs), which are the anchor key technology for bringing plasmonics to a feasible experimental platform for light manipulation. One of the frequently studied types of one-dimensional (1D) PCs consists of metal-dielectric gratings supporting the diffraction-induced SPPs excitation according to the quasiphase-matching conditions

$$\mathbf{k}_{\mathrm{SPP}} = \mathbf{k}_{\parallel} + m\mathbf{G}, \tag{2}$$

where $\mathbf{k}_{\parallel}$ is the tangential component of the wave vector of the incident wave, $\mathbf{G}$ is the reciprocal lattice vector of the grating, and m is the diffraction order. Renaissance of optics of metallic gratings is spurred by many breakthroughs in the field of control of the SPP waves in PCs [13]. The PCs conquered the realm of photonics for their potential in molecular and refractive index sensors [12,14], enhancement of Raman scattering [15], biosensors [16], optical modulators, and switches [17,18].

Recently we have witnessed fascinating enhancement of the magneto-optical effects in the PCs embodied magnetic materials [19]. It fuels the interest to these structures, dubbed magnetoplasmonic crystals (MPCs), in which the plasmonic and magneto-optical effects are intertwined. This MPC property was leveraged for the design of precise magnetic field sensors [20–22], nonreciprocal plasmonic devices [23], and refractive index change sensors [24–26]. These promising applications became possible owing to the resonant increase of the Faraday effect [23,27], transverse [28,29] and longitudinal magneto-optical Kerr effect (MOKE) [30], and diffracted magneto-optical effect [31], to name but a few, demonstrated in the MPCs under the SPP excitation.

Of particular interest are the MPCs based on the magnetic dielectrics like iron garnets marveled for their magneto-optical response and relatively high transparency [29,32,33]. Being combined with a grating made of noble metal possessing small optical losses in the visible spectral range, these MPCs exhibit high-quality SPP resonances suitable for precise optical applications [20]. Magnetization of a medium comprising the MPC gives an exquisite way to control the SPP dispersion, thus giving a valuable transverse magneto-optical Kerr effect (TMOKE), which is manifold enhanced as compared to the out-of-the-SPP resonance

*vb.novikov@physics.msu.ru

 ©2022 American Physical Society

conditions [34]. Besides, extra functionalities are introduced by the presence of the waveguide modes in the magnetic dielectric layer adjacent to the grating leading to the enhancement of the light-matter interaction [35] and giving rise to a novel longitudinal magnetophotonic intensity effect suitable for the magnetic field-induced modulation of light [36,37].

A huge plasmonic-assisted enhancement of optical fields inspires the efforts towards the intensification of the nonlinear phenomena in plasmonics structures [34,38]. Since the pioneering works demonstrating a distinct increase of the optical second harmonic generation (SHG) in metal films owing to the SPPs excitation [39,40], various plasmonic structures were applied to increase a wide range of the nonlinear optical effects. In particular, the enhancement of the second [41,42] and third harmonic generation [43,44], as well as the four-wave mixing [45], were achieved in plasmonic gratings. An additional boost of the optical effects is achieved in hybrid plasmon-photonic structures [46]. Moreover, magnetic structures can support magnetization-induced modulation of the SHG intensity that exceeds linear magneto-optical effects by several orders of magnitude [47–49]. This makes nonlinear magneto-optics highly attractive for sensing and magnetic field-driven control of light [38,50] and attracts attention to nonlinear magneto-optics of plasmonic structures [35,38,48,51,52].

Special attention is attributed to the MPCs based on a combination of ferromagnetic and noble metals providing the high quality SPP resonances and a strong magneto-optical activity, which greatly exceeds that of magnetic dielectrics. The SPP-driven increase of the TMOKE was implemented for MPCs of various designs, based on single uniform ultrathin films of ferromagnetic metals like nickel, iron, and cobalt covering dielectric gratings [21,30,53,54]. An improved magneto-optical response of MPCs is achieved in structures with a ferromagnetic layer juxtaposed with gold or silver periodic gratings [22,24,25,28,55–58] or squeezed between a couple of noble metal films [28,59]. Significant endeavors were applied to enhance magneto-optical effects in perforated hybrid gold/cobalt gratings [26,27] harnessing the extraordinary optical transmission [60–62]. Alternative realized MPC designs were based on arrays of ferromagnetic disks and stripes [30,53,63,64], or plasmonic structures located on a ferromagnetic substrate [65]. Additional functionality could be achieved as well due to harnessing bright and dark plasmonic modes [5,66] or the presence of additional modes except SPP ones, e.g., Mie plasmons supported by the metallized inverse opals [67].

Besides ferromagnetic metals as iron, cobalt, and nickel applied prominently for the fabrication of MPCs, special attention is paid to permalloy (Py), which is a soft ferromagnetic nickel-iron alloy ($Ni_{80}Fe_{20}$) [68]. This material is promising for a wide range of applications owing to the superior magnetic properties including high Curie temperature, small magnetic anisotropy, coercitivity, Gilbert damping, and magnetostriction, which inspires the application of Py in spintronic devices [69] as well as for the realization of room temperature skyrmion states [70]. The bind of Py and PCs demonstrates a strong potential for the magneto-optical applications and sensing [21,53,56,65,71–74], as well as magnetic control over the photoinduced electric voltage as was demonstrated quite recently [75].

Recently curved geometries of magnetic materials have attracted a lot of attention inspired by myriads of nontrivial magnetic states in these systems [76,77] promising for the spintronics applications. Engineering of magnetic nanostructures results in the curvature-induced magnetochirality [78], skyrmions, magnetic vortices, helical states in spherical surfaces, and nanotubes [79–81] to name a few. Even in thin films the curvature can be the source of magnetic anisotropy [82]. In spite of the impressive progress in the studies of the shape effects in magnetic properties of various structures, the investigations of SPP-mediated optical effects in the MPCs with nonuniform magnetization have not been performed to the best of our knowledge.

In this work we investigate the SPP-driven enhancement of the TMOKE and of the second harmonic generation in a MPC composed of gold and Py ultrathin films deposited on a 1D dielectric grating. We demonstrate both experimentally and theoretically that in the conical light diffraction geometry, the magnetic anisotropy of the corrugated ferromagnetic layer is of crucial importance for the appearance of magneto-optical effects and can be considered as an additional way for the control over the magneto-optical effects in MPCs. The paper is organized as follows. In Sec. II we provide the parameters of the considered MPC structures along with their magneto-optical properties, description of the experimental procedures, and the obtained results. In Sec. III we discuss the details of simulations and results of calculations of linear and nonlinear diffraction of light in the MPCs. The Conclusions section finalizes the paper.

II. EXPERIMENTAL DETAILS

A. Experimental structure

In this work the experimental studies of resonant effects in magneto-optical and second-harmonic response of MPC are carried out for a 1D metal-dielectric surface-relief grating. The spatial profile of the structure unit cell is shown in Fig. 1(a). The grating was obtained in the following way. First, a $500 \times 500\,\mu$m 1D array of dielectric ridges made of the hydrogen silsesquioxane (HSQ) resist was formed by electron-beam lithography on a quartz substrate. The grating period was $d = 600$ nm, ridge height was 63 nm, and its width was 70 nm. Then the resist pattern was covered by a 6-nm-thick adhesive Ti layer with the subsequent deposition of gold and permalloy films with the thicknesses of $d_{\mathrm{Au}} = 80$ nm, $d_{\mathrm{Py}} = 10$ nm; permalloy being a ferromagnetic alloy introduces magneto-optical activity to the MPC. The value d_{Au} is chosen to bury the dielectric grating forming the periodic surface relief. The thickness of the ferromagnetic layer (d_{Py}) is justified to provide alignment of the magnetization along corrugated Py thin film [82] and minimize the effect of the formation of islands under the sputtering process. The SEM image of the upper surface of the grating is demonstrated in Fig. 1(b). For convenience we denote the upper gold interface as "1" and the bottom one as "2," as indicated in Fig. 1(a).

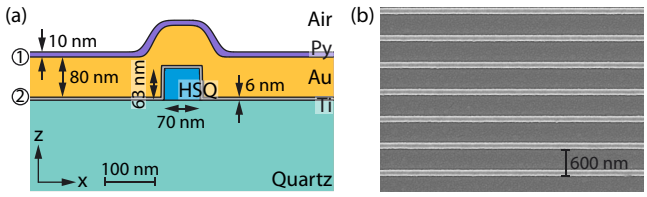

FIG. 1. (a) Scheme of the unit cell of the grating. Circled numbers indicate the interfaces of the gold film. (b) SEM image of the grating.

B. Magneto-optical properties of permalloy

Magneto-optical effects originate from the appearance of nondiagonal components of the permittivity tensor of a magnetized material

$$\hat{\varepsilon} = \begin{pmatrix} \varepsilon & ig_z & -ig_y \\ -ig_z & \varepsilon & ig_x \\ ig_y & -ig_x & \varepsilon \end{pmatrix}, \tag{3}$$

where ε is the diagonal permittivity component of an isotropic material, $\mathbf{g} = (g_x, g_y, g_z)$ is the gyration vector proportional to the magnetization $\mathbf{M}$, i.e., $\mathbf{g} = \alpha\mathbf{M} = g(\mathbf{M})\mathbf{m}$, $\mathbf{m} = \mathbf{M}/M$ is a unit vector [83]. Here we adopted $\varepsilon = \varepsilon' + i\varepsilon''$ and $g = g' + ig''$ and assume the $\exp(-i\omega t)$ convention for the optical fields [84].

We found a strong easy-plane magnetic anisotropy of a flat 10-nm-thick permalloy film, which appears as a strong difference in the parameters of the hysteresis loops measured in the transverse and polar magneto-optical Kerr effects that is typical for ultrathin magnetic films [85,86]. For these studies, a reference Py film was made in the same deposition cycle on a flat substrate (without a dielectric grating). In that case the in-plane coercivity is rather small, $H_c^{\parallel} = 20$ Oe, in agreement with previous measurements [72,85,87]. In turn, for the out-of-plane direction the magnetic saturation was not achieved up to $H = 4.5$ kOe that corresponds to previous studies of the magnetization of 10 nm Py film, which saturates at $H \approx 10$ kOe [85], that is 500 times larger than $H_c^{\parallel}$.

To estimate the spectral dependence of the complex g value in the case of permalloy, we proposed a dual-measurement method based on the analysis of the spectra of the TMOKE and polar magneto-optical effect (PMOKE). In these experiments, the p-polarized light of a halogen lamp was incident at the angle of $\theta = 22.5^\circ$ on the reference flat Au/Py film. The in-plane transverse and out-of-plane DC magnetic field with the strength of about 3.5 and 4 kOe, respectively, formed by permanent neodymium magnets were applied. Reversal of the magnetic field direction was realized by rotating the magnets by 180°; this allowed us to measure the TMOKE magnetic contrast given by

$$\rho_t = \frac{I(\mathbf{M}) - I(-\mathbf{M})}{I(\mathbf{M}) + I(-\mathbf{M})}, \tag{4}$$

which describes the relative change of the reflected light intensity (I) under the magnetization reversal when p-polarized light is incident and an analyzer is absent. The obtained TMOKE spectrum ρ_t for the Au/Py film is shown by the black curve in Fig. 2(a). When studying the PMOKE consisting of odd in magnetization rotation of the polarization plane and ellipticity change of the reflected light, we set the incident

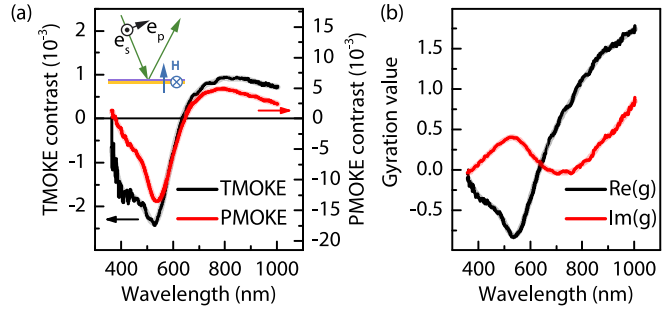

FIG. 2. (a) Measured spectra of the magnetic contrast of the transverse (ρ_t) and polar (ρ_p) MOKE for Au/Py film deposited on a flat quartz substrate. Inset: Geometry of light incidence and basis vectors of the optical polarization. (b) Extracted spectra of the Py complex gyration value.

light polarization at the angle $\psi = -45^\circ$ with respect to the p polarization, so that its electric field is described by $\mathbf{E}_{\text{inc}} = \mathbf{e}_p \cos(\psi) + \mathbf{e}_s \sin(\psi)$ [inset in Fig. 2(a)], while the analyzer selected the s-polarized reflected light. The spectrum of the magnetic contrast ρ_p of the PMOKE determined similarly to Eq. (4) is shown by a red curve in Fig. 2(a). The most pronounced PMOKE occurring near $\lambda = 540$ nm corresponds to the rotation of the major axis of the polarization ellipse up to 0.4° at the structure magnetization. We have to stress that for an applied combination of polarizations the values of ρ_t and ρ_p of the transverse and polar MOKE never become zero simultaneously until $g = 0$, which allowed us to estimate the complex value of g.

Using the transfer-matrix method adapted for anisotropic multilayers, we reconstructed the spectra of Re(g) and Im(g) of permalloy from ρ_t and ρ_p spectra; the corresponding dependencies are shown in Fig. 2(b). One can see that the real part of the gyration value of permalloy changes its sign near the wavelength $\lambda = 630$ nm and reveals a valuable growth of its real and imaginary parts with increasing λ. As well, real and imaginary parts of g reveal local extrema near $\lambda = 540$ nm.

C. SPP resonances in light reflection from MPC

The investigations of the resonant optical effects in MPCs were carried out in conical diffraction geometry, as illustrated in Fig. 3(a). The angle of incidence of the probe beam was $\theta = 22.5^\circ$, and the plane of incidence was oriented at the azimuth angle φ with respect to the grating periodicity direction as shown in Fig. 3(a). For convenience we introduce two coordinate frames [Fig. 3(a)]. The first one, XYZ, is related to the MPC with the x axis parallel to the periodicity direction of the grating. The second one, X′Y′Z, is rotated by φ with respect to the XYZ coordinate system, with the x' axis lying in the plane of incidence. The utilized conical diffraction geometry is known to give additional degree of freedom for the light interaction with diffraction gratings, which was applied in the polarization converters [88], biosensors [89], and is scarcely mentioned in magneto-optics [54,64]. In our linear-optical experiments, the p- or s-polarized light beam of a halogen lamp was focused into a 100×50 μm spot by a lens with $f = 5$ cm to the MPC and the reflected radiation was detected by an Avesta ASP-75 spectrometer in the wavelengths range

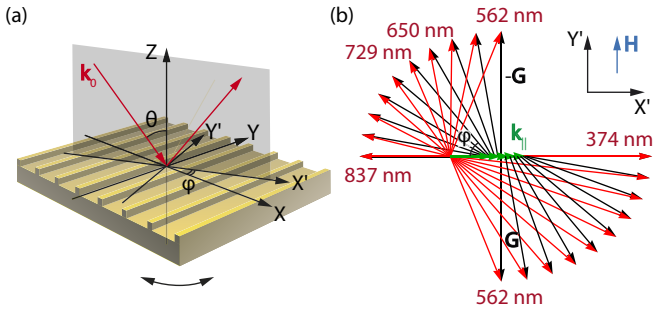

FIG. 3. (a) Scheme of the light incidence upon the MPC. (b) Wave-vector diagram of the diffraction assisted excitation of SPP given by Eq. (2) for various light wavelengths, $\varphi = 0°$–$90°$ and diffraction orders $m = \pm 1$. Green arrows are $\mathbf{k}_{||}$, red ones are $\mathbf{k}_{spp}$, and black ones are $\pm\mathbf{G}$.

of 400–1000 nm. The convergence angle of the incident light was about $\delta\theta = 1°$ which had the negligible effect of about 3% in the smearing of the SPP features of the MPC. The MPC reflection spectra were normalized to those of the flat Au/Py reference film.

Figure 4 shows the experimental reflection spectra of the MPC for various azimuth angles φ, for p and s polarizations of the incident light. One can see that the reflection coefficient of the MPC reveals spectral minima, which are missing for flat Au/Py film and are shifting towards shorter wavelengths when φ tends to $\pm 90°$. For the p-polarized light, the most pronounced features are observed in the spectral range of 600–900 nm. In the case of the s polarization, there are several sets of minima. We address the first one lying in the same range of λ as for the p polarization and additional ones in the near-infrared (IR) range of $\lambda > 920$ nm. The typical spectral width of the resonances observed in the range $\lambda = 600$–900 nm is about $\Delta\lambda = 40$ nm, their strength being strongly dependent on the incident angle: for the p polarization it decreases at detuning φ from zero, while for the s polarization the minimum is the most pronounced at $\varphi = \pm 50°$ and $\pm 90°$, and

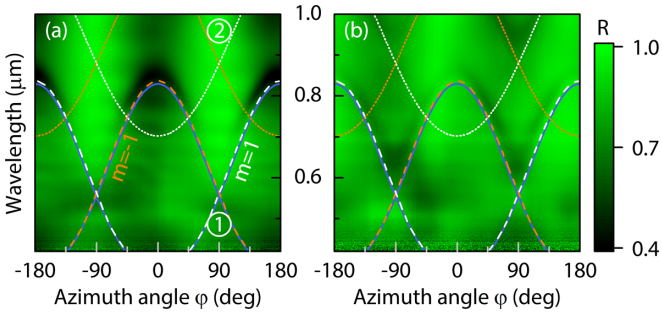

FIG. 4. Experimental λ-φ spectra of the reflectance of MPC for (a) p-polarized and (b) s-polarized light. The reflection coefficient is normalized to that of the reference Au/Py film. Quasisynchronism conditions for the SPP excitation at the MPC interfaces 1 and 2 [determined by Eqs. (2) and (5)] are shown by dashed and dotted curves, respectively; the interface number is shown in the circle. The diffraction orders $m = -1$ ($m = 1$) are indicated by orange (white). Solid blue curves indicate the Rayleigh anomalies corresponding to the diffraction orders $m = \pm 1$ for the air interface of the grating.

disappears for $\varphi = 0°$. We note that the local decrease of the light reflection of both the MPC and the flat multilayer film near the wavelength of 490 nm caused by the interband transitions in gold disappears under normalization to the reflectance of the reference Au/Py film (Supplemental Material Sec. I [90]).

We address the observed resonant optical features of MPC to the diffraction-assisted SPP excitation in the grating. To illustrate this we overlay (i) λ-φ curves of the Rayleigh anomaly attributed to the diffracted order oriented along the grating surface and (ii) the SPP dispersion curves in Fig. 4. The former ones obtained for interface 1 according to $k_0 = |\mathbf{k}_{||} + m\mathbf{G}|$ with the diffraction orders $m = \pm 1$ are shown by blue curves in Fig. 4. The SPP dispersion curves for $m = \pm 1$ were obtained using Eq. (2) where $k_{\mathrm{SPP}}(\lambda)$ for the flat SiO_2/Ti/Au/Py/Air multilayer film was calculated by solving the following equation:

$$\det \hat{M}(\lambda, k_x) = 0, \tag{5}$$

with respect to k_x, where the matrix $\hat{M}$ expresses the boundary conditions of the continuity of the tangential components of electric and magnetic fields of the light waves at the film interfaces [91]. A similar approach is commonly used for dispersion analysis of guided modes and surface waves in metamaterials [92,93]. We note that the obtained SPP curves are very close to ones driven by a combination of Eqs. (1) and (2) that is justified by a small thicknesses of Py and Ti layers juxtaposed to thick Au film. As seen, the obtained SPP dispersion reproduces quite well the spectral shift of the resonances with the azimuth rotation of the grating. The λ-φ dependence of the Rayleigh anomaly shown in Fig. 4 appears for shorter wavelengths than the SPP dispersion curves (dashed curves) and observed reflection minima, sustaining the SPP origin of the latter. The calculations show that the main reflection minima are attributed to the SPP whose field is localized predominantly near interface 1 of the Au film, while the near-IR ones observed for the s polarization of light at $\lambda > 920$ nm [Fig. 4(b)] are related to the SPP excitation at interface 2 [Fig. 1(a)].

D. Linear transverse magneto-optical Kerr effect

Let us consider the magneto-optical response of the MPC. The measurements of the TMOKE were performed by the procedure similar to that used in Sec. II B. In the experiment the magnetic field with the strength of $H = 2$ kOe oriented along y' axis was applied, i.e., it was lying in the structure plane perpendicularly to the plane of incidence [Fig. 3(a)]. In this static magnetic field the MPC was rotated around the z axis. The obtained spectra of the TMOKE contrast for the p- and s-polarized incident light are shown in Fig. 5. One can see that a broadband nonzero magnetic contrast is revealed under the reflection of the p-polarized light from the MPC, the typical value of the magnetic contrast is $\rho_t \sim 10^{-3}$ in the near-IR. It is accompanied by the sign change of ρ_t in the vicinity of $\lambda = 600$ nm [Fig. 5(a)], which stems from the magneto-optical spectrum of permalloy gyration value shown in Fig. 2(b).

At the same time we revealed that the considered MPC sustains SPP-assisted resonant enhancement of the TMOKE.

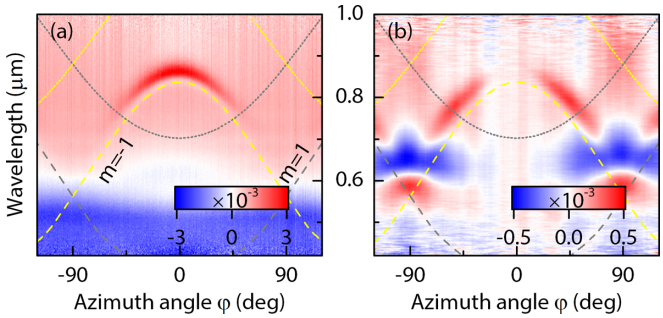

FIG. 5. Experimental λ-φ TMOKE spectra of the MPC for (a) *p*- and (b) *s*-polarized incident light. Quasisynchronism conditions [Eqs. (2) and (5)] for the excitation of SPP at interfaces 1 (dashed curve) and 2 (dotted curve) of the MPC for the diffraction orders $m = -1$ ($m = 1$) indicated by yellow (gray).

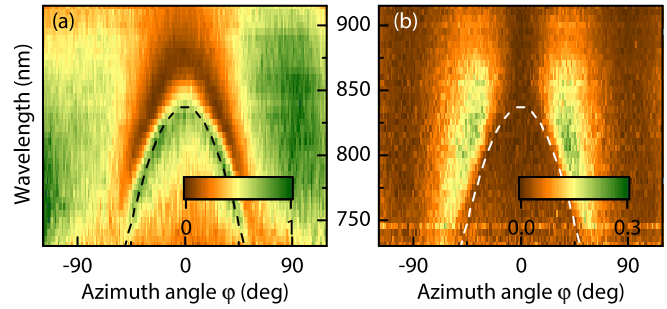

FIG. 6. Experimental λ-φ map of the power of (a) *p*-polarized and (b) *s*-polarized components of the reflected SHG. Labels of the wavelength axis correspond to the fundamental radiation. Dashed curves correspond to the SPP dispersion.

For the *p* polarization of the probe light, a pronounced narrowband resonant growth of ρ_t is observed, its position at the λ-φ map matches well the minimum of the MPC reflection [Fig. 5(a)]. The peak value of the magnetic contrast $\rho_t = 3 \times 10^{-3}$ is approximately three times larger than for the reference flat Au/Py film. Interestingly that the sign of the magnetic contrast in the vicinity of SPP resonance is not changed and the enhancement of ρ_t as well as resonant reflection minimum is rather symmetric with respect to φ and λ, contrary to asymmetric Fano-like resonant contours with the sign reversal of ρ_t observed in other types of MPCs [24,29]. As seen, the variation of the azimuth angle φ from the zero value causes a decrease of ρ_t along the SPP dispersion curve, which is caused by the lowering of the SPP amplitude and the strength of the reflection minimum [Fig. 4(a)]. It is worth noting that the TMOKE enhancement takes place solely for SPP localized at interface 1 of the grating that is caused by the proximity of the ferromagnetic film to this interface.

In the case of the *s*-polarized light, the TMOKE of the MPC is about one order of magnitude smaller than that attained for the *p* polarization [Fig. 5(b)] and reaches maximum values of the magnetic contrast of $\rho_t = 3 \times 10^{-4}$ close to the SPP resonant curve, while for flat Au/Py film ρ_t is zero within the experimental accuracy in accordance with the expectations [83]. Curiously, contrary to that, the MPC demonstrates spectral broadband nonzero TMOKE in the near-IR near $\varphi = 90°$ for *s*-polarized light that stems from the surface relief of the grating. In contrast to the results for the *p*-polarized light, there is no enhancement of ρ_t at $\varphi = 0°$ [Fig. 5(b)], which results from the prohibition for the SPP excitation by the *s*-polarized light when the SPP wave vector $\mathbf{k}_{SPP}$ is in the plane of incidence. We address special attention to the threefold sign change of the TMOKE contrast close to $\varphi = 90°$ for *s*-polarized light [Fig. 5(b)]. As is discussed below, this peculiarity is a fingerprint of the specific in-plane magnetization of the corrugated ferromagnetic layer covering the grating.

E. Second harmonic generation in MPC

Second harmonic generation in MPC was studied in the same geometry as the linear MOKE [Fig. 3(a)]. In the experiments, a Ti-Sa laser generating the pulses with the duration of 60 fs and repetition rate of 80 MHz tunable in the spectral range of 730–915 nm was used as the light source. As seen in Fig. 4, in this spectral range the SPP is excited efficiently by the *p*-polarized incident light that was used in SHG experiments. The fundamental beam with the mean power of $P = 15$ mW was focused by a $f = 5$ cm lens upon the MPC into a spot with the diameter of about $d = 17$ μm, the angle of incidence was $\theta = 22.5°$. The convergence angle of incident light was about $\delta\theta = 3°$ corresponding to the broadening factor of the SPP resonant dip of about 1.25. The second harmonic (SH) radiation generated in reflection from the grating was extracted by an appropriate set of color filters and detected by a photomultiplier operating in the photon counting mode. The Glan prizm analyzer was used for the selection of *p*- and *s*-polarized SH components.

Figure 6 shows the wavelength-azimuth angle maps of the power of *p*- and *s*-polarized SH components generated in reflection from the MPC. First, we stress a strong effect of the SPP excitation at interface 1 at the fundamental frequency on the nonlinear response. Second, we address the broadband *p*-polarized SHG, which takes place almost in the whole range of the azimuth angle φ [Fig. 6(a)] and corresponds to the SHG allowed at the interfaces, the main SHG contribution being due to the $\chi^{(2)}_{zzz}$ term of the surface nonlinear susceptibility [94,95]. In contrast, the generation of the *s*-polarized SH wave is prohibited at flat interfaces of isotropic media, while we observed weaker but nonzero *s*-polarized SHG [Fig. 6(b)], originating from the surface relief of the grating and the SPP excitation.

The SPP excitation in MPC appears in different ways in the generation of *p*- and *s*-polarized SHG components. In the first case, SPP excitation leads to the coexistence of a deep minimum adjacent to a maximum of the SHG power, their spectral position in a λ-φ map matches well to the SPP-induced minimum of the linear reflection [Fig. 4(a)]. Thus close to the SPP resonances, the Fano-like spectral line of the SH signal is formed. In contrast to the case of the *p*-polarized SHG, the generation of the *s*-polarized SH wave is strongly enhanced in the spectral-angular region matching the resonant SPP excitation [Fig. 6(b)].

High SPP-driven sensitivity of the SHG to the magnetic state of the MPC is demonstrated in Fig. 7, which shows the experimental azimuth dependencies of the power of the *p*-polarized component of the reflected SH radiation and

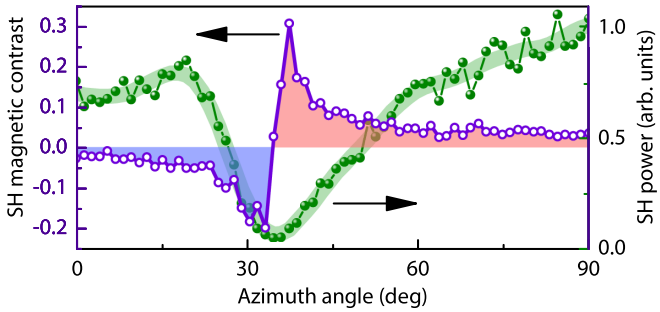

FIG. 7. Azimuth dependencies of the reflected p-polarized SHG power and of its magnetic contrast measured under the excitation of the MPC by the p-polarized fundamental radiation at $\lambda = 820$ nm.

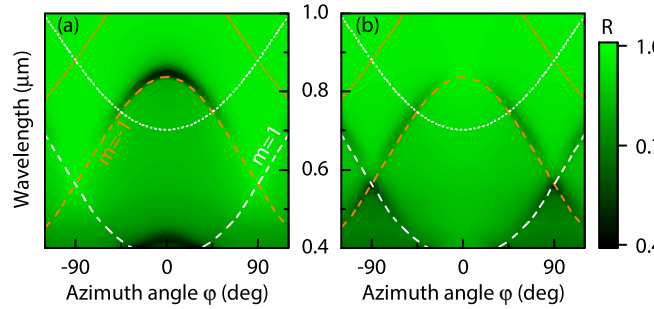

FIG. 8. Calculated λ-φ spectra of the relative reflectance of MPC for (a) p-polarized and (b) s-polarized light. The reflection coefficient is normalized to one of the flat Au/Py films. Dispersion curves [Eqs. (2) and (5)] for excitation of SPP on interfaces 1 (dashed curve) and 2 (dotted curve) of the MPC. Diffraction order $m = -1$ ($m = 1$) is indicated by orange (white).

its magnetic contrast when the MPC is illuminated by the p-polarized fundamental radiation at $\lambda = 820$ nm. As can be seen, resonant enhancement of the magnetic contrast up to the value of 30% takes place within the SPP resonance contour, accompanied by the sign reversal of the nonlinear TMOKE. The maximal contrast value is 10–15 times larger than its nonresonant value and is two orders of magnitude larger than the linear TMOKE. It can be noted that strong values of nonlinear MOKE up to 5×10^{-2} were demonstrated in the magnetic granular films [96]. Under the attenuated total reflection the uniform iron films resulted in nonlinear ρ of about 20% [49]. Our results agree with revealed earlier the SPP-mediated enhancement of the nonlinear MOKE in other types of MPC [48,51,97] and uniform three-layer Au/Co/Au plasmonic films [98] demonstrating up to several dozens percent nonlinear MOKE accompanied by the sign change of ρ near the SPP excitation conditions.

III. NUMERICAL SIMULATIONS AND DISCUSSION

A. Linear optics of MPC

In order to corroborate the revealed SPP-induced phenomena in the optical response of MPC we carried out numerical simulations of linear and nonlinear diffraction of light in this structure harnessing the finite element method (FEM) through the application of COMSOL software. We applied the spatial profile of the unit cell of the surface-relief grating shown in Fig. 1(a). To emulate the infinite-size structure, Floquet periodic boundaries were imposed in the x and y directions, while perfectly matched layers (PMLs) were used in vertical (z) direction. The calculations were carried out in the frequency domain for a convenient incorporation of the spectral dependencies of the dielectric permittivities of constituent materials taken from Refs. [99,100]. In all simulations the angle of incidence was taken as in the experiment, $\theta = 22.5^\circ$, while the azimuth angle φ and light wavelength λ were varied. The stability of the numerical results to the parameters of the computational domain and PML, especially near the wavelengths of the Rayleigh anomaly, was confirmed by auxiliary simulations.

The obtained λ-φ dependencies of the reflection coefficients for p- and s-polarized light normalized to the reflection spectra of a flat film are shown in Fig. 8. They stay in a good agreement with the results of the experiments shown in Fig. 4. The calculated MPC reflection spectra exhibit the minima with their spectral position corresponding to the SPP dispersion curves given by Eqs. (2) and (5) for $m = \pm 1$ and shown by dashed lines in Fig. 8. For s polarization of light the most pronounced features associated with the SPP excitation take place at $\varphi = \pm 55^\circ$–60° and $\pm 90^\circ$, while for the p-polarized light it occurs at $\varphi = 0^\circ$ similarly to the experimental results (Figs. 8 and 4).

We assert that revealed sensitivity of the SPP excitation with respect to the azimuth angle in the vicinity of $\varphi = 0^\circ$ results from the mismatch of the directions of the electric field vectors of the incident wave $\mathbf{E}_{\text{inc}}$ and SPP $\mathbf{E}_{\text{SPP}}$. Indeed, the applied conical geometry of light diffraction from the grating leads to the SPP propagation in the direction out of the plane of incidence. This is illustrated by Fig. 3(b), where the diagram of the Bragg excitation of the SPP at the MPC interface 1 is shown for various λ and diffraction orders $m = \pm 1$ (this vector scheme in XYZ frame attributed to the grating is shown in the Supplemental Material Fig. 2 [90]). This scheme corresponds to the dashed dispersion curves in the range $\varphi = 0^\circ$–90° in Fig. 8. It shows that the SPP wave vector $\mathbf{k}_{\text{SPP}}$ could be even orthogonal to the incidence plane as it takes place for $\lambda = 650$ nm [Fig. 3(b)]. The most efficient SPP excitation takes place when $\langle \mathbf{E}_{\text{inc}} \mathbf{E}_{\text{SPP}} \rangle$ is maximal as it occurs at $\varphi = 0^\circ$ for the p polarization of the incident light.

Numerical studies of the TMOKE spectra were performed when taking the dielectric permittivity of the Py film in the tensor form [Eq. (3)], with the complex gyration value $g(\lambda)$ estimated in the experiment [see Fig. 2(b)]. Special attention was paid to the orientation of the gyration vector $\mathbf{g} = g(\lambda)\mathbf{m}$ of the Py layer under the application of the static magnetic field $\mathbf{H}$ along the OY′ direction, i.e., oriented at the angle φ with respect to the MPC stripes. To untangle the origin of the experimentally revealed threefold sign change of the TMOKE spectrum at the azimuth angle $\varphi = 90^\circ$ [Fig. 5(b)], we proposed that the direction of the Py magnetization $\mathbf{m}$ is affected by the profile of the grating. Instead of the uniform magnetization when $\mathbf{m} = \mathbf{H}/H$, as a matter of fact, we assumed $\mathbf{m}$ to be along the Py layer following the film bending, i.e., unit vector is $\mathbf{m} = [\mathbf{n} \times [\mathbf{H} \times \mathbf{n}]]/\|\mathbf{m}\|$, where $\mathbf{n}$ is the outward normal vector to the Py film. We refer this type of the magnetization

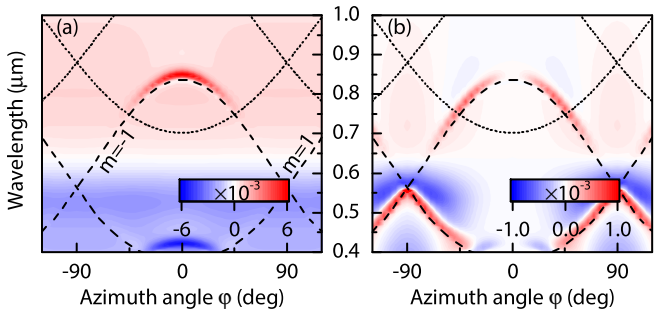

FIG. 9. Calculated λ-φ spectra of TMOKE for (a) *p*- and (b) *s*-polarized light. Dashed (dotted) curves are the dispersion curves of SPP localized at interface 1 (2).

as in-plane. This is illustrated schematically for $\varphi = 90^\circ$ in the right inset of Fig. 10. This model is justified by a strong magnetic shape anisotropy of a few-nm-thick ferromagnetic films for which the saturation of the out-of-plane magnetization could be achieved at the magnetic field with strength of several kOe [85,86]. For 10-nm-thick Py film it occurs for $H \approx 10$ kOe [85] manifold exceeding the saturation field for the in-plane directions in accordance with our observations (Sec. II B). The alignment of the magnetic moments along the corrugated thin film was demonstrated in Refs. [82,101] and originates from the minimization of the magnetostatic energy.

The calculated TMOKE spectra shown in Fig. 9 for both polarization states of the incident light demonstrate pronounced SPP-driven resonant features of TMOKE in agreement with the experimental results (Fig. 5). Similar to the experiment, an increase of the TMOKE occurs in the spectral vicinity of the dispersion curves of the order $m = \pm 1$ for SPP confined by interface 1, while far from these resonances nonzero TMOKE exists driven by the magneto-optical response of the Py film. In turn, the nonzero TMOKE for *s*-polarized light beyond the SPP excitation is caused by the interplay of (i) the corrugation of the ferromagnetic layer resulting in the mixed polarization of the incident light in local regions of the ridge's walls and (ii) in-plane permalloy magnetization. As for *p* polarization, the enhancement

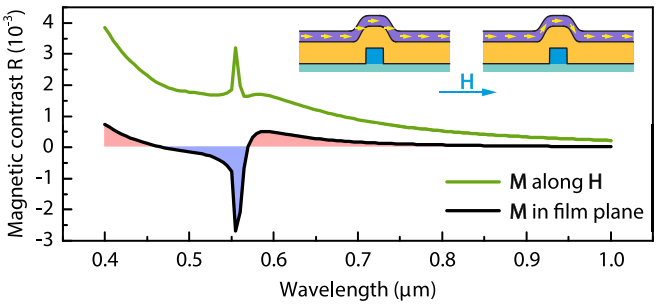

FIG. 10. Comparison of the calculated spectra of the TMOKE in the MPC for *s*-polarized light incident at $\varphi = 90^\circ$ for the Py layer magnetized along **H** (green curve) and along the film (black curve). The gyration value of permalloy is taken dispersionless and equal to $g = 1$. Inset demonstrates by yellow arrows both cases of magnetization profile of Py film.

of TMOKE for *s*-polarized incident light appears near the diffraction-assisted excitation of the SPP.

We stress the decisive role of the in-plane magnetization in conspicuous manifold sign change in the TMOKE spectrum for *s*-polarized light near $\varphi = 90^\circ$ and $\lambda = 600$ nm revealed experimentally [see Fig. 5(b)]. We affirm that it is in-plane magnetization of the grating cover layer that gives a sign change of TMOKE spectra even for dispersionless gyration value g, which is not the case of the uniform magnetization. It is demonstrated explicitly in Fig. 10, which illustrates the calculated TMOKE for both types of magnetization of the Py layer in the MPC when *s*-polarized light is incident at $\varphi = 90^\circ$. To make the effect of the magnetization type on the magnetic contrast more obvious, in these calculations the dispersion of the Py gyration value was neglected and we took $g = 1$. One can see that in-plane magnetization of the MPC structure gives the change of the TMOKE sign (black curve) contrary to the uniform **M** when the TMOKE does not experience it (green curve). Revealed effect gives rise to a pronounced TMOKE enhancement under the SPP excitation by *s*-polarized light for $\lambda < 600$ nm [Figs. 9(b) and 5(b)]. To the best of our knowledge, the intertwine of the SPPs and the nonuniform magnetization in MPCs is found for the first time. We emphasize that the nonuniform magnetization is decisive not only for resonant, but also for off-resonant TMOKE spectrum. This makes the TMOKE with the *s*-polarized light a sensitive probe of magnetization of the corrugated ferromagnetic films. It is sustained as well by the robustness of the revealed effect to the roughness of gold and permalloy films. It was confirmed by the additional simulations involving the random perturbation of the interfaces with the root-mean-square roughness of $R_q = 3$ nm, which is even larger than $R_q = 1.5$ nm for the experimental structure. We emphasize that the propagation of the SPPs in MPC out of the plane of light incidence that is mediated by the conical diffraction enriches the magneto-optical effects, which can be further intensified by tuning the direction of **H** with respect to the SPP wave vector.

B. Second harmonic generation

Numerical simulations were carried out for the SHG in plasmonic grating under the SPP excitation in the undepleted pump approximation by executing the two coupled simulations attributed to the (i) fundamental and (ii) SH fields, within the FEM in the frequency domain. First, the spatial distribution of the electric field of the fundamental radiation inside the grating was determined under the incidence of the *p*-polarized plane wave upon the MPC. Then it was recasted to the spatial distribution of the vectorial nonlinear polarization considered as the light source in the subsequent simulation of SHG.

The second-order response of the structure raises from the surface and bulk second-order nonlinearities of a metal, i.e., its nonlinear polarization is given by [102,103]

$$\mathbf{P}^{\mathrm{NL}} = \mathbf{P}^{\mathrm{NL}}_{\mathrm{surf}} + \mathbf{P}^{\mathrm{NL}}_{\mathrm{bulk}}. \tag{6}$$

The last term is attributed to the gas of free (conductive) electrons, and its nonlocal nonlinear polarization in the frame of the hydrodynamic model [104–106] takes the form

$$\mathbf{P}^{\mathrm{NL}}_{\mathrm{bulk}} = \alpha \nabla(\mathbf{E}\cdot\mathbf{E}) + \beta(\mathbf{E}\cdot\nabla)\mathbf{E}. \tag{7}$$

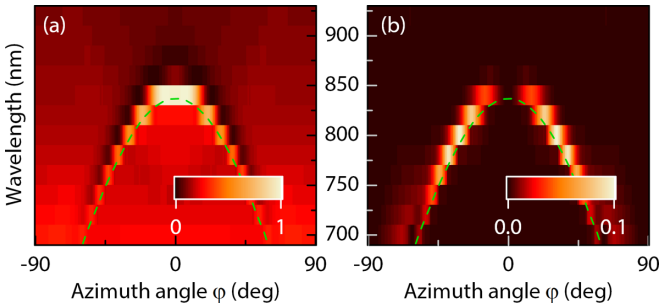

FIG. 11. Calculated λ-φ dependencies of the power of (a) *p*- and (b) *s*-polarized SHG components. Dashed curve is the dispersion curve of SPP localized at interface 1.

Recently it was shown that the bulk nonlinearity of metal is of paramount importance for the second-order response of plasmonic nanostructures [106–108]. Our simulations confirm that it is $\mathbf{P}^{\mathrm{NL}}_{\mathrm{bulk}}$ that gives a qualitative agreement of the numerical results with the experimental ones, while the $\mathbf{P}^{\mathrm{NL}}_{\mathrm{surf}}$ is insufficient and we skip it in the calculations. The second term in Eq. (7) disappears in homogeneous media and gives a very weak SH response of the considered grating as compared to SHG driven by the first term. For this reason we employed ultimately the nonlinear polarization in the form of $\mathbf{P}^{\mathrm{NL}} = \alpha\nabla(\mathbf{E}\cdot\mathbf{E})$.

The results of the calculations of the power of *s*- and *p*-polarized SHG in reflection from the MPC as a function of λ and φ for the *p* polarization of the fundamental beam are shown in Fig. 11. Obtained maps demonstrate salient features similar to the experimental ones (Fig. 6). We would like to underline that it is the nonlocal bulk nonlinear response of metal which gives rise to Fano-like resonant enhancement of *p*-polarized SHG under the SPP excitation [Fig. 11(a)]. In turn, the surface nonlinearity driven predominantly by $\chi^{(2)}_{\perp\perp\perp}$ [94,95] leads to the increase of *p*-polarized SHG without a minimum specific to the Fano line.

The results of the calculations also show that the SHG under the SPP excitation in the conical diffraction geometry contains a quite intense *s*-polarized SH wave for $\varphi \neq 0^\circ$ [Fig. 11(b)] that is in agreement with the experimental data [Fig. 6(b)]. We attribute this effect to the asymmetric interaction of light with the gratings when both the plane of incidence and the direction of propagation of the diffraction-induced SPP are inclined with respect to the grating ridges.

IV. CONCLUSION

To summarize, in this work we carried out the experimental investigation of the resonant enhancement of linear and nonlinear TMOKE as well as the SHG in the conical diffraction geometry in the MPC based on gold and permalloy films covering the periodic dielectric grating. The structure is inspired by bridging together a well pronounced SPP resonance sustained by gold and significant magneto-optical activity of the ferromagnetic layer. We revealed SPP-driven enhancement of the TMOKE, which appears for both *s* and *p* polarizations of the incident light in contrast to the usual diffraction geometry when diffracted beams are in the incidence plane and the TMOKE is zero for *s*-polarized light. We elucidated the crucial role of the effect of in-plane magnetization of Py layer in the TMOKE for the symmetric geometry of light interaction when the grating ridges are in the incidence plane. This magnetization type results in the sign of SPP-driven TMOKE opposite the one for the case of the uniform magnetization of the ferromagnetic film. Our findings intertwine the SPP and the nonuniform magnetization that is useful for its probing and can be promising for the intensification of other magneto-optical effects. The explicit Fano-like resonance in the SHG attributed to the SPP excitation is manifested experimentally and confirmed by numerical simulations. The revealed effect is accompanied by pronounced *s*-polarized SHG induced by the SPP excitation at the conical diffraction of fundamental radiation. A decisive role of the bulk second-order nonlinearity of metal constituent of the grating in this nonlinear process is found by numerical calculations. Demonstrated resonant effects in the SH response are accompanied by valuable nonlinear TMOKE achieving 30% associated with the SPP excitation at the fundamental frequency.

ACKNOWLEDGMENTS

This work was supported by the Russian Foundation for Basic Research, Project No. 19-02-00826. Samples of plasmonic crystals were produced using the material and technical resources of the BMSTU Nanofabrication Facility (FMN Laboratory, FMNS REC, ID 74300). SEM images were recorded using equipment of the Educational and Methodological Center for Lithography and Microscopy, Faculty of Physics, Moscow State University. A.M.R. acknowledges the financial support of the Theoretical Physics and Mathematics Advancement Foundation "BASIS".

[1] S. Celiksoy, W. Ye, K. Wandner, K. Kaefer, and C. Sönnichsen, Nano Lett. **21**, 2053 (2021).
[2] K. Kneipp, M. Moskovits, and H. Kneipp, Phys. Today **60**(11), 40 (2007).
[3] S. David, C. Polonschii, C. Luculescu, M. Gheorghiu, S. Gáspár, and E. Gheorghiu, Biosens. Bioelectron. **63**, 525 (2015).
[4] A. I. Väkeväinen, R. J. Moerland, H. T. Rekola, A.-P. Eskelinen, J.-P. Martikainen, D.-H. Kim, and P. Törmä, Nano Lett. **14**, 1721 (2014).
[5] T. Hakala, H. Rekola, A. Väkeväinen, J.-P. Martikainen, M. Nečada, A. Moilanen, and P. Törmä, Nat. Commun. **8**, 13687 (2017).
[6] R. H. Ritchie, Phys. Rev. **106**, 874 (1957).
[7] S. A. Maier, *Plasmonics: Fundamentals and Applications* (Springer, New York, 2007)
[8] G. I. Stegeman, R. F. Wallis, and A. A. Maradudin, Opt. Lett. **8**, 386 (1983).
[9] C. Fisher, L. C. Botten, C. G. Poulton, R. C. McPhedran, and C. M. de Sterke, J. Opt. Soc. Am. B **32**, 412 (2015).

[10] E. Kretschmann and H. Raether, Z. Naturforsch. Teil A. **23**, 2135 (1968).

[11] A. Otto, Z. Phys. A: Hadrons Nucl. **216**, 398 (1968).

[12] Y. Xu, P. Bai, X. Zhou, Y. Akimov, C. E. Png, L.-K. Ang, W. Knoll, and L. Wu, Adv. Opt. Mater. **7**, 1801433 (2019).

[13] W. L. Barnes, A. Dereux, and T. W. Ebbesen, Nature (London) **424**, 824 (2003).

[14] L. Li, X. Zong, and Y. Liu, J. Phys. D **53**, 185106 (2020).

[15] J. J. Baumberg, T. A. Kelf, Y. Sugawara, S. Cintra, M. E. Abdelsalam, P. N. Bartlett, and A. E. Russell, Nano Lett. **5**, 2262 (2005).

[16] J. Homola, *Surface Plasmon Resonance Based Sensors* (Springer Science & Business Media, New York, 2006), Vol. 4.

[17] X. Zhang and J. Yang, Front. Phys. **7**, 190 (2019).

[18] G. Wang, H. Lu, X. Liu, and Y. Gong, Nanotechnology **23**, 444009 (2012).

[19] N. Maccaferri, I. Zubritskaya, I. Razdolski, I.-A. Chioar, V. Belotelov, V. Kapaklis, P. M. Oppeneer, and A. Dmitriev, J. Appl. Phys. **127**, 080903 (2020).

[20] G. A. Knyazev, P. O. Kapralov, N. A. Gusev, A. N. Kalish, P. M. Vetoshko, S. A. Dagesyan, A. N. Shaposhnikov, A. R. Prokopov, V. N. Berzhansky, A. K. Zvezdin, and V. I. Belotelov, ACS Photonics **5**, 4951 (2018).

[21] V. Belyaev, D. Murzin, N. Perova, A. Grunin, A. Fedyanin, and V. Rodionova, J. Magn. Magn. Mater. **482**, 292 (2019).

[22] V. K. Belyaev, V. V. Rodionova, A. A. Grunin, M. Inoue, and A. A. Fedyanin, Sci. Rep. **10**, 7133 (2020).

[23] J. Y. Chin, T. Steinle, T. Wehlus, D. Dregely, T. Weiss, V. I. Belotelov, B. Stritzker, and H. Giessen, Nat. Commun. **4**, 1599 (2013).

[24] B. F. Diaz-Valencia, J. R. Mejía-Salazar, O. N. Oliveira, N. Porras-Montenegro, and P. Albella, ACS Omega **2**, 7682 (2017).

[25] A. A. Grunin, I. R. Mukha, A. V. Chetvertukhin, and A. A. Fedyanin, J. Magn. Magn. Mater. **415**, 72 (2016).

[26] B. Caballero, A. García-Martín, and J. C. Cuevas, ACS Photonics **3**, 203 (2016).

[27] B. Caballero, A. García-Martín, and J. C. Cuevas, Opt. Express **23**, 22238 (2015).

[28] C. Clavero, K. Yang, J. R. Skuza, and R. A. Lukaszew, Opt. Lett. **35**, 1557 (2010).

[29] V. Belotelov, I. Akimov, M. Pohl, V. Kotov, S. Kasture, A. Vengurlekar, A. V. Gopal, D. Yakovlev, A. Zvezdin, and M. Bayer, Nat. Nanotechnol. **6**, 370 (2011).

[30] A. Chetvertukhin, A. Grunin, A. Baryshev, T. Dolgova, H. Uchida, M. Inoue, and A. Fedyanin, J. Magn. Magn. Mater. **324**, 3516 (2012), fifth Moscow international symposium on magnetism.

[31] R. Cichelero, M. Kataja, M. Campoy-Quiles, and G. Herranz, Opt. Express **26**, 34842 (2018).

[32] A. L. Chekhov, V. L. Krutyanskiy, V. A. Ketsko, A. I. Stognij, and T. V. Murzina, Opt. Mater. Express **5**, 1647 (2015).

[33] A. L. Chekhov, P. N. Naydenov, M. N. Smirnova, V. A. Ketsko, A. I. Stognij, and T. V. Murzina, Opt. Express **26**, 21086 (2018).

[34] M. Kauranen and A. V. Zayats, Nat. Photonics **6**, 737 (2012).

[35] V. L. Krutyanskiy, A. L. Chekhov, V. A. Ketsko, A. I. Stognij, and T. V. Murzina, Phys. Rev. B **91**, 121411(R) (2015).

[36] V. I. Belotelov, D. A. Bykov, L. L. Doskolovich, A. N. Kalish, V. A. Kotov, and A. K. Zvezdin, Opt. Lett. **34**, 398 (2009).

[37] V. Belotelov, L. Kreilkamp, I. Akimov, A. Kalish, D. Bykov, S. Kasture, V. Yallapragada, A. V. Gopal, A. M. Grishin, S. I. Khartsev *et al.*, Nat. Commun. **4**, 2128 (2013).

[38] W. Zheng, X. Liu, A. T. Hanbicki, B. T. Jonker, and G. Lüpke, Opt. Mater. Express **5**, 2597 (2015).

[39] H. J. Simon, D. E. Mitchell, and J. G. Watson, Phys. Rev. Lett. **33**, 1531 (1974).

[40] C. K. Chen, A. R. B. de Castro, and Y. R. Shen, Opt. Lett. **4**, 393 (1979).

[41] A. L. Chekhov, I. Razdolski, A. Kirilyuk, T. Rasing, A. I. Stognij, and T. V. Murzina, Phys. Rev. B **93**, 161405(R) (2016).

[42] G. F. Walsh and L. Dal Negro, Nano Lett. **13**, 3111 (2013).

[43] S. Chen, W. Wong, Y. Pun, K. Cheah, and G. Li, Adv. Opt. Mater. **1**, 522 (2013).

[44] S. Chen, G. Li, F. Zeuner, W. H. Wong, E. Y. B. Pun, T. Zentgraf, K. W. Cheah, and S. Zhang, Phys. Rev. Lett. **113**, 033901 (2014).

[45] B. Jin and C. Argyropoulos, Sci. Rep. **6**, 28746 (2016).

[46] V. B. Novikov, A. A. Nasonov, A. Maydykovskiy, and T. V. Murzina, JETP Lett. **108**, 296 (2018).

[47] A. Kirilyuk and T. Rasing, J. Opt. Soc. Am. B **22**, 148 (2005).

[48] D. Newman, M. Wears, R. Matelon, and D. Mchugh, Appl. Phys. B **74**, 719 (2002).

[49] W. Zheng, A. T. Hanbicki, B. T. Jonker, and G. Lüpke, Opt. Express **21**, 28842 (2013).

[50] W. Zheng, A. T. Hanbicki, B. T. Jonker, and G. Lüpke, Sci. Rep. **4**, 6191 (2014).

[51] I. Razdolski, S. Parchenko, A. Stupakiewicz, S. Semin, A. Stognij, A. Maziewski, A. Kirilyuk, and T. Rasing, ACS Photonics **2**, 20 (2015).

[52] I. Razdolski, D. Makarov, O. G. Schmidt, A. Kirilyuk, T. Rasing, and V. V. Temnov, ACS Photonics **3**, 179 (2016).

[53] N. Kostylev, I. S. Maksymov, A. O. Adeyeye, S. Samarin, M. Kostylev, and J. F. Williams, Appl. Phys. Lett. **102**, 121907 (2013).

[54] A. A. Grunin, A. G. Zhdanov, A. A. Ezhov, E. A. Ganshina, and A. A. Fedyanin, Appl. Phys. Lett. **97**, 261908 (2010).

[55] Q. Wang, H. Yao, Y. Feng, X. Deng, B. Yang, D. Xiong, M. He, and W. Zhang, Opt. Express **29**, 10546 (2021).

[56] A. R. Pomozov, A. L. Chekhov, I. A. Rodionov, A. S. Baburin, E. S. Lotkov, M. P. Temiryazeva, K. N. Afanasyev, A. V. Baryshev, and T. V. Murzina, Appl. Phys. Lett. **116**, 013106 (2020).

[57] S. A. Dyakov, I. M. Fradkin, N. A. Gippius, L. Klompmaker, F. Spitzer, E. Yalcin, I. A. Akimov, M. Bayer, D. A. Yavsin, S. I. Pavlov, A. B. Pevtsov, S. Y. Verbin, and S. G. Tikhodeev, Phys. Rev. B **100**, 214411 (2019).

[58] I. Kolmychek, A. Romashkina, A. Maydykovskiy, S. Gusev, N. Gusev, M. Sapozhnikov, V. Golubev, and T. Murzina, JETP Lett. **114**, 456 (2021).

[59] V. V. Temnov, G. Armelles, U. Woggon, D. Guzatov, A. Cebollada, A. Garcia-Martin, J.-M. Garcia-Martin, T. Thomay, A. Leitenstorfer, and R. Bratschitsch, Nat. Photonics **4**, 107 (2010).

[60] T. W. Ebbesen, H. J. Lezec, H. Ghaemi, T. Thio, and P. A. Wolff, Nature (London) **391**, 667 (1998).

[61] V. I. Belotelov, D. A. Bykov, L. L. Doskolovich, A. N. Kalish, and A. K. Zvezdin, J. Opt. Soc. Am. B **26**, 1594 (2009).

[62] V. I. Belotelov, L. L. Doskolovich, and A. K. Zvezdin, Phys. Rev. Lett. **98**, 077401 (2007).

[63] A. V. Chetvertukhin, A. A. Grunin, T. V. Dolgova, M. Inoue, and A. A. Fedyanin, J. Appl. Phys. **113**, 17A942 (2013).

[64] V. Novosad, Y. Souche, V. Pishko, T. Crozes, Y. Otani, and K. Fukamichi, IEEE Trans. Magn. **35**, 3145 (1999).

[65] T. H. J. Loughran, P. S. Keatley, E. Hendry, W. L. Barnes, and R. J. Hicken, Opt. Express **26**, 4738 (2018).

[66] A. Y. Frolov, M. R. Shcherbakov, and A. A. Fedyanin, Phys. Rev. B **101**, 045409 (2020).

[67] A. A. Grunin, N. A. Sapoletova, K. S. Napolskii, A. A. Eliseev, and A. A. Fedyanin, J. Appl. Phys. **111**, 07A948 (2012).

[68] H. D. Arnold and G. W. Elmen, Bell Syst. Tech. J. **2**, 101 (1923).

[69] G. Nahrwold, J. M. Scholtyssek, S. Motl-Ziegler, O. Albrecht, U. Merkt, and G. Meier, J. Appl. Phys. **108**, 013907 (2010).

[70] R. Streubel, L. Han, M.-Y. Im, F. Kronast, U. K. Rößler, F. Radu, R. Abrudan, G. Lin, O. G. Schmidt, P. Fischer, and M. Denys, Sci. Rep. **5**, 8787 (2015).

[71] V. Novikov, A. Romashkina, D. Ezenkova, I. Rodionov, K. Afanas'ev, A. Baryshev, and T. Murzina, Opt. Spectrosc. **128**, 1481 (2020).

[72] D. Kulikova, K. Afanasyev, I. Bykov, S. Efremova, A. Pomozov, E. Shalygina, and A. Baryshev, Opt. Mater. (Amsterdam) **107**, 110067 (2020).

[73] D. V. Murzin, V. K. Belyaev, F. Groß, J. Gräfe, M. Rivas, and V. V. Rodionova, Jpn. J. Appl. Phys. **59**, SEEA04 (2020).

[74] V. G. Kravets, P. Y. Kurioz, and L. V. Poperenko, J. Opt. Soc. Am. B **31**, 1836 (2014).

[75] M. Shahabuddin, D. W. Keene, M. Durach, V. S. Posvyanskii, V. A. Atsarkin, and N. Noginova, J. Opt. Soc. Am. B **38**, 2012 (2021).

[76] R. Streubel, P. Fischer, F. Kronast, V. P. Kravchuk, D. D. Sheka, Y. Gaididei, O. G. Schmidt, and D. Makarov, J. Phys. D **49**, 363001 (2016).

[77] R. Streubel, E. Y. Tsymbal, and P. Fischer, J. Appl. Phys. **129**, 210902 (2021).

[78] R. Hertel, *Spin* (World Scientific, Singapore, 2013), Vol. 3, p. 1340009.

[79] R. Streubel, D. Makarov, F. Kronast, V. Kravchuk, M. Albrecht, and O. G. Schmidt, Phys. Rev. B **85**, 174429 (2012).

[80] V. P. Kravchuk, D. D. Sheka, R. Streubel, D. Makarov, O. G. Schmidt, and Y. Gaididei, Phys. Rev. B **85**, 144433 (2012).

[81] H. D. Salinas, J. Restrepo, and Ò. Iglesias, Sci. Rep. **8**, 10275 (2018).

[82] M. O. Liedke, M. Körner, K. Lenz, M. Fritzsche, M. Ranjan, A. Keller, E. Čižmár, S. A. Zvyagin, S. Facsko, K. Potzger, J. Lindner, and J. Fassbender, Phys. Rev. B **87**, 024424 (2013).

[83] A. K. Zvezdin and V. A. Kotov, *Modern Magnetooptics and Magnetooptical Materials* (CRC, Boca Raton, FL, 1997).

[84] R. Atkinson and P. H. Lissberger, Appl. Opt. **31**, 6076 (1992).

[85] T. Jin, M. Ranjbar, S. He, W. Law, T. Zhou, W. Lew, X. Liu, and S. Piramanayagam, Sci. Rep. **7**, 16208 (2017).

[86] G. Yang, X. Xing, O. Obi, A. Daigle, M. Liu, S. Stoute, K. Naishadham, and N. Sun, IET Microwaves Antennas Propag. **4**, 1172 (2010).

[87] A. V. Svalov, I. R. Aseguinolaza, A. Garcia-Arribas, I. Orue, J. M. Barandiaran, J. Alonso, M. L. FernAndez-Gubieda, and G. V. Kurlyandskaya, IEEE Trans. Magn. **46**, 333 (2010).

[88] N. Passilly, K. Ventola, P. Karvinen, P. Laakkonen, J. Turunen, and J. Tervo, Appl. Opt. **46**, 4258 (2007).

[89] S. Rossi, E. Gazzola, P. Capaldo, G. Borile, and F. Romanato, Sensors **18**, 1621 (2018).

[90] See Supplemental Material at http://link.aps.org/supplemental/10.1103/PhysRevB.105.155408 for (i) a discussion of the effect of interband transition in gold on the light reflection from the magnetoplasmonic crystal and flat film, and (ii) wave-vector diagrams of the diffraction-assisted excitation of the SPP in the coordinate system of the grating.

[91] H. Baltar, K. Drozdowicz-Tomsia, and E. M. Goldys, Propagating surface plasmons and dispersion relations for nanoscale multilayer metallic-dielectric films, in *Plasmonics: Principles and Applications*, edited by K. Y. Kim (InTech, 2012), Chap. 6, pp. 136–155.

[92] E. Snitzer, J. Opt. Soc. Am. **51**, 491 (1961).

[93] V. B. Novikov and T. V. Murzina, AIP Conf. Proc. **2300**, 020091 (2020).

[94] F. X. Wang, F. J. Rodríguez, W. M. Albers, R. Ahorinta, J. E. Sipe, and M. Kauranen, Phys. Rev. B **80**, 233402 (2009).

[95] D. Krause, C. W. Teplin, and C. T. Rogers, J. Appl. Phys. **96**, 3626 (2004).

[96] T. V. Murzina, E. A. Ganshina, S. V. Guschin, T. V. Misuryaev, and O. A. Aktsipetrov, Appl. Phys. Lett. **73**, 3769 (1998).

[97] I. Razdolski, D. G. Gheorghe, E. Melander, B. Hjörvarsson, P. Patoka, A. V. Kimel, A. Kirilyuk, E. T. Papaioannou, and T. Rasing, Phys. Rev. B **88**, 075436 (2013).

[98] G. Tessier and P. Beauvillain, Appl. Surf. Sci. **164**, 175 (2000).

[99] M. N. Polyanskiy, Refractive index database, database https://refractiveindex.info.

[100] K. K. Tikuišis, L. Beran, P. Cejpek, K. Uhlířová, J. Hamrle, M. Vaňatka, M. Urbánek, and M. Veis, Mater. Design **114**, 31 (2017).

[101] C. A. F. Vaz, S. J. Steinmuller, and J. A. C. Bland, Phys. Rev. B **75**, 132402 (2007).

[102] J. Butet, P.-F. Brevet, and O. J. F. Martin, ACS Nano **9**, 10545 (2015).

[103] J. I. Dadap, J. Shan, and T. F. Heinz, J. Opt. Soc. Am. B **21**, 1328 (2004).

[104] N. Bloembergen, R. K. Chang, S. S. Jha, and C. H. Lee, Phys. Rev. **174**, 813 (1968).

[105] J. E. Sipe, V. C. Y. So, M. Fukui, and G. I. Stegeman, Phys. Rev. B **21**, 4389 (1980).

[106] Y. Zeng, W. Hoyer, J. Liu, S. W. Koch, and J. V. Moloney, Phys. Rev. B **79**, 235109 (2009).

[107] N. Feth, S. Linden, M. W. Klein, M. Decker, F. B. P. Niesler, Y. Zeng, W. Hoyer, J. Liu, S. W. Koch, J. V. Moloney, and M. Wegener, Opt. Lett. **33**, 1975 (2008).

[108] B. Wells, A. Y. Bykov, G. Marino, M. E. Nasir, A. V. Zayats, and V. A. Podolskiy, Optica **5**, 1502 (2018).